Mechanics & Industry **20**, 602 (2019)
© AFM, EDP Sciences 2019
https://doi.org/10.1051/meca/2019017

Mechanics & Industry

Available online at:
www.mechanics-industry.org

Regular Article

Design and shape optimization of MR brakes using Nelder–Mead optimization algorithm

Yousef Bazargan-Lari*

Department of Mechanical Engineering, Shiraz Branch, Islamic Azad University, Shiraz, Iran

Received: 3 January 2018 / Accepted: 8 March 2019

Abstract. Magnetorheological (MR) brakes have attracted many attentions for controlling mechanical systems such as robots, e-bicycles, and haptic devices. A large number of researchers have delved into enhancing MR brake effectiveness. Herein, a new MR brake is proposed in which the braking torque is improved and the configuration is simplified. Numerical simulations were based on finite element method (FEM) was employed to achieve the brake model. In order to verify the obtained results, they were compared with the available ones in the literature and they have a good agreement with each other. Then, the proper brake model was optimized using Nelder–Mead optimization algorithm. Results demonstrated 215.75 N m braking torque in the present prototype which is almost 73% higher than the previous model in the literature. In addition, the brake could induce about 125.06 N m torque on the brake disk with nearly half of the coil current used in the previous work. Besides, increase in the number of the disks was not necessarily improved braking efficiency and the size of the MR fluid gaps also influenced the brake operation. In addition, the proposed model in this paper has ease manufacturing procedure which would reduce the fabrication costs.

Keywords: Brake system / MR brake / MR fluid / optimization / Nelder–Mead algorithm / FEM

1 Introduction

Breakthroughs in technology have made it possible for researchers to synthesize materials with controllable properties. These smart materials are sensitive to external stimuli sources such as heat source, magnetic, or electric fields and their properties like their size or solidity are changed [1]. Magnetorheological (MR) fluid is one type of smart materials with variable viscosity in external magnetic fields which is synthesized using magnetizable micro/nanoparticles suspended in a base fluid. The particles are attracted to each other aligned with the magnetic field and generate some strong metallic chains in the base fluid which change the fluid to a semi-solid structure [2,3]. The fast and reversible response of these fluids to the external magnetic fields is highly desirable for employing in mechanical systems such as dampers [4], breaks [5], clutches [6], hydraulic valves [7], and polishing devices [8]. Brakes are the vital section in the mechanical systems with moving parts. They perform based on friction [9], electro-magnetic [10], hydraulic or mechanical coupling [11] between two different machines and hinder movement by harnessing the energy of moving segments [12]. The essential role of brake systems for handling mechanical devices has urged scholars to study different types of brakes. Generally, these MR brakes consisted from an immersed disk in an MR fluid within an enclosure and the magnetic field was induced around the MR fluid by a coil. When the brake operated, the magnetic field led to changing the MR fluid to semi-solid condition. Consequently, yield stress and shear friction were increased on the disk surface and reduced the speed [13].

Recently, the MR brakes have attracted the attentions for utilizing in various devices such as haptic joystick [14], haptic glove [15], e-bicycle [16], and robots [17,18]. For instance, Lee et al. [17] employed rotary MR brake for controlling robotic ankle motion and optimized the prototype using genetic algorithm. Besides, they considered temperature effects on the performance of the brake. Lee et al. [17] utilized MR brake system to control tension of a rope in winch spooler system. First, they designed and simulated the system by FEM, then they fabricated and tested the most optimized configuration. Senkal and Gurocak [14] presented a haptic joystick which had a two degree of freedom actuator constructed from a spherical MR-brake and three air muscles. In addition to these applications, MR brakes have been widely designed for automotive brake system and various influential parameters on the braking operation were investigated. For example, Sarkar and Hirani [19] suggested that wave form edge for the brake disk enhanced its efficiency. Among

* e-mail: bazarganlari@iaushiraz.ac.ir

different studied wave shapes, they proved that a disk with parabolic waves on its edge resulted in higher braking torque. Park et al. [20] studied the effects of magnetostatics, fluid flow, and heat transfer on the braking efficiency of an MR brake with a single disk. Furthermore, they optimized the model and the most efficient configuration was suggested. Assadsangabi et al. [21] employed FEM to model a novel MR brake with double disk and optimized the brake system by genetic algorithm. Zhou et al. [22] proposed an MR brake system with two rotating disks immersed in MR fluid. They suggested that this configuration could produce large torques in small radial dimensions and they proved it by fabrication of their design. Wang et al. [23] studied an MR brake systems with multiple disks. In order to reduce the generated heat in the brake, they employed water circulation around the brake. Wang et al. [24] studied the effects of surface textures of the disk on the braking performance. They built three disks with different surface textures and test them experimentally. Their results proved that a disk with square surface texture had more friction torque than other texture shapes. Lydia et al. [25] investigated the effects of coil shape on an MR brake operation. Their results proved that a trapezoidal coil with angle between 60° and 70° resulted in higher magnetic torque in the brake. Lijesh et al. [13] investigated the effects of disk hardness on the MR brake performance. Their empirical results demonstrated that particles in the MRF destroyed disks with soft surfaces and reduce performance of the brake. They reduced this undesirable effect by hardening the surface of the disk. Patil et al. [16] designed an MR brake for an e-bicycle brake. They considered the effects of temperature on the braking operation and demonstrated that their designed brake worked within an acceptable temperature range. Younis et al. [26] used SEUMRE algorithm to optimize an MR brake system. The main objective of their study was demonstrating the application of this algorithm for highly nonlinear and sophisticated engineering design optimization problems. Moreover, they compared the results of this algorithm with genetic (GA) and simulated annealing (SA) algorithms.

In the present numerical paper, a new configuration for the MR brake disk of reference [21] is proposed which enhances the braking torque about 73%. The present brake disk configuration also has more simplified fabrication procedure. In order to verify the simulation results, the brake in reference [21] was simulated and the results were in a good agreement with each other. Then, different disks were simulated and the most efficient and simple one was optimized using Nelder–Mead optimization algorithm. The rest of the paper is organized as follows. The next section devotes for describing the materials and methods. The obtained results are presented in Section 3 and finally, in Section 4 concluding remarks are proposed.

2 Materials and methods

2.1 MR fluid

The main employed materials to build an MR brake are stainless steel and MR fluid. Among different proposed MR fluids, MRF-132DG fluid is the material of choice by researchers due to its fast response time, temperature resistant, higher deposition time, and non-abrasive features [27]. Yield stress of this fluid is a function of magnetic field and Bingham plastic model is the most appropriate estimation to show this relationship (Eq. (1)).

Table 1. MRF-132DG properties [28].

Property	MRF-132DG
Base fluid	Hydrocarbon
Operating temperature	−40 to 130 °C
Density	3.09 g/cc
Viscosity	0.09 (±0.02) Pa s
k	0.269 Pa m/A
β	1

$$\tau = \tau_y(H) + \mu_p \dot{\gamma} \tag{1}$$

where $\tau_y(H)$ (N/m^2) represents yield stress due to the applied magnetic field ($H(T)$), μ_p (Pa s) is constant plastic viscosity, which is considered equal to the no-field viscosity of the fluid, and $\dot{\gamma}$ (1/s) is the shear–strain rate. For a rotating disk $\dot{\gamma}$ is [20,21]:

$$\dot{\gamma} = \frac{r\omega}{\delta} \tag{2}$$

where r (m) is the radius of the disk, ω (Rad/s) is the angular velocity, and δ (m) is the MR fluid gap. Besides, $\tau_y(H)$ derives from [20,21]:

$$\tau_y(H) = kH^{\beta} \tag{3}$$

where $H(T)$ represents the magnetic field intensity. Also, k and β are the parameters which estimate relationship between magnetic field intensity and yield stress. For MRF-132DG these constants along with other properties are shown in Table 1 [28].

2.2 Magnetic field

The magnetic flux distribution is obtained from Maxwell–Ampere law as follows:

$$\nabla \times \mathrm{H} = \mathbf{J} \tag{4}$$

where $\mathbf{J}$ is the current density (A/m^2), and $\mathbf{H}$ is the magnetic field (T) and the relation between the magnetic field and magnetic flux is:

$$\mathbf{B} = \mu_0 \mu_r \mathrm{H} \tag{5}$$

where μ_0 (N/A^2) is free space permeability and μ_r is relative permeability of material. B–H curve of materials can used in order to find $\mu_0\mu_r$ constant. Therefore, B–H curves of steel 1018 and MRF-132DG are employed here for

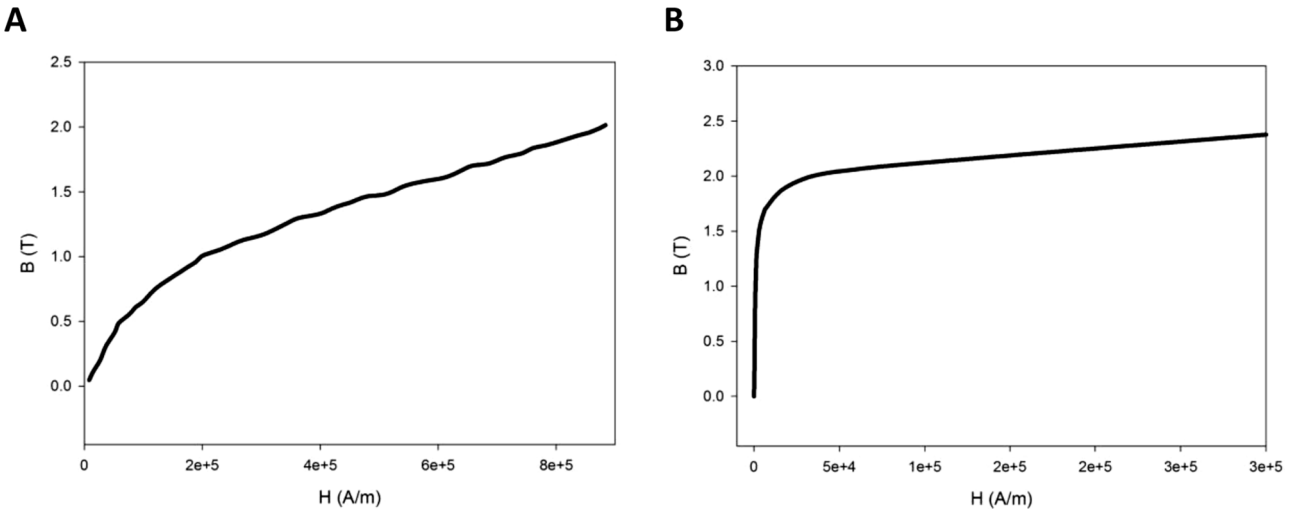

Fig. 1. *B-H* curves for: (a) MRF-132DG [29], (b) steel 1018 [21].

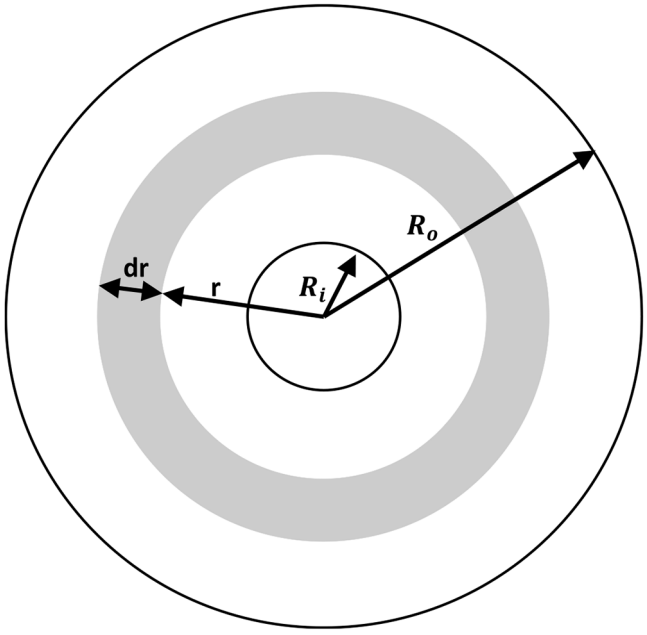

Fig. 2. Surface element on the disk for integration of shear stress.

this purpose (Fig. 1) [21,29]. Such strategy was widely utilized by previous researchers to simulate MR brakes [20–22,28–32].

2.3 Induced torque

The total torque generated from shear stress on the disk shown in Figure 2 is calculated from:

$$\mathrm{T} = \int r\tau dA = 2\pi n \int_{R_i}^{R_0} r^2 \tau dr \tag{6}$$

The applied torque on the disk is mainly induced by the magnetic field (T_m (N m)) and the fluid viscosity (T_η (N m)).

These components are:

$$T_m = 2\pi n \int_{r_i}^{r_0} kH^\beta r^2 dr \tag{7}$$

$$T_\eta = \frac{\pi}{2\delta} n\mu_\mathrm{p}\omega(R_0^4 - R_i^4) + \pi n R_0^2 \tau_\eta t. \tag{8}$$

The radius component of the magnetic field intensity (**H**) is small at the end of the disk faces, so its effects is negligible on the exerted torque [21]. Many researchers employed 2-D axisymmetric numerical simulation to find magnetic field distribution on the disk and employed equation (7) to calculate the induced magnetic field torque on the disk [16,17,21,22,30,31,33–35].

2.4 Nelder–Mead optimization algorithm

Optimization methods are employed to select the most efficient value from several choices. A large number of optimization algorithms such as genetic algorithm [21,31], SEUMRE [26], and multidisciplinary design optimization (MDO) [28] were employed in order to reach the best configuration of MR brakes. These algorithms search based on different methods. One of the most time efficient method is applying Heuristic technique to gain an approximate solution for a problem. In this context, the optimum value (maximum or minimum) of the objective is found by searching in a space. Genetic algorithms, swarm intelligence, and artificial neural networks method are some of the algorithms which search based on heuristic technique [36,37]. Besides, Nelder and Mead [38] also

presented an optimization algorithm that quite simple to implement. The general steps of optimization with this algorithm are [39]:
- Initialize the simplex;
- Sort vertices and compute centroid;
- Update the worst vertex or shrink simplex.

2.5 Numerical method

The abovementioned system of equations was solved using COMSOL Multiphysics. This software works based on FEM and the most interesting feature of this package is modeling of different coupled physics in one case without using any extra coupling methods [40–43]. In this method, the partial differential equations (PDEs) are reduced to a set of algebraic equations. The modeling domain is divided into smaller parts called the elements and the dependent variables are represented by polynomial shape functions over these elements. Then, these variables are substituted in the governing PDEs and a weighted integral of these equations is taken over the element. Consequently, the result depicted as a set of algebraic equations for the variables on the elements [41]. MUltifrontal Massively Parallel sparse direct Solver (MUMPS) is employed in order to solve this coupled PDEs. This solver has been employed to calculate large linear algebraic equation systems and it can work out-of-core solution storing which makes it possible to use more memory than the available memory on the computers [44].

In the present paper, triangular elements were used to discrete the computational domain. Since the simulations were based on FEM, it was necessary to demonstrate that the obtained results were independent of the number of elements. The grid independent test was done for all the models. As an example, 11 593 number of elements were used to assure that the obtained results from the simulations of the model shown in Figure 3A were independent from the number of grids.

3 Result and discussions

3.1 Validation

Assadsangabi et al. [21] presented an MR brake in their investigation (Fig. 3A). In order to verify the validity of present numerical simulation, this model was simulated. Table 2 represents the dimensions of this brake. As the electric current flows through the coil wires, the magnetic field applies to the MR fluid, the shear stress increases on the disk and stops the disk from rotating. Figure 3B shows distribution of z component of magnetic flux density ($\mathbf{H}z$) and Figure 3C shows distribution of z component of magnetic field intensity ($\mathbf{B}z$). These distributions are in a good agreement with the presented results by Assadsangabi et al. [21]. Also, they mentioned that their proposed MR brake produced 126.54 N m magnetic torque and 5.35 N m viscous torque on the disk [21]. The numerical results of the present study also showed that the magnetic torque was 125.02 N m and the viscous torque was obtained about 5.88 N m. Therefore, the present numerical procedure had enough accuracy to investigate MR brakes.

Table 2. Optimum dimensions of the MR break [21].

Variables	Values
$d1$	0.505 m
$d2$	0.1811 m
$d3$	0.0013 m
$d4$	0.003 m
$d5$	0.0148 m
$d6$	0.0122 m
$d7$	0.0063 m
$d8$	0.0183 m
a	0.5
b	0.35

3.2 Proposed disk arrangements

After verifying the validity of the employed numerical method, different layouts of the brake disk were considered to find their effectiveness (Fig. 4). It should be noted that weight of the proposed layouts was the main constraint in selection and the weight of these models were the same. The generated magnetic torques of these configurations are shown in Table 3.

According to Table 3, in the same conditions, the disk with the configuration shown in Figure 4C induced higher magnetic torque to stop the brake. The results also demonstrated that increase in the number of disks, such as Figure 4D, did not result in the brake efficiency enhancement. And the depth of the MR fluid cuts also affected the braking operation. Moreover, distance between the cuts in Figure 4C was also changed to find whether the position of these cuts had any effects on the braking efficiency or not. Figure 5A shows magnetic torque of different positions of these cuts. According to this figure, when the distance between cuts increased, the magnetic torque first decreased, but then increased again. Figure 5B shows distribution of z component of magnetic flux density (Hz) and Figure 5C shows distribution of z component of magnetic field intensity (Bz) for the brake with two cuts in the distance of 0.0163 m from each other. According magnetic field distribution, when the cuts machined near the edge of the disk, the magnetic field had higher density and resulted in magnetic torque enhancement. To illustrate, the new layout shown in Figure 5B could produce magnetic torque of 125.06 N m with nearly half of the coil current of the MR brake model of Figure 3A.

3.3 Optimization

According to the result, the configuration of Figure 4C was optimized in order to find the dimensions in which the magnetic torque was maximum. The results of the previous section illustrated distance between the cuts as well as their width and depth affected the induced magnetic torque on the brake disk. Consequently, these parameters were

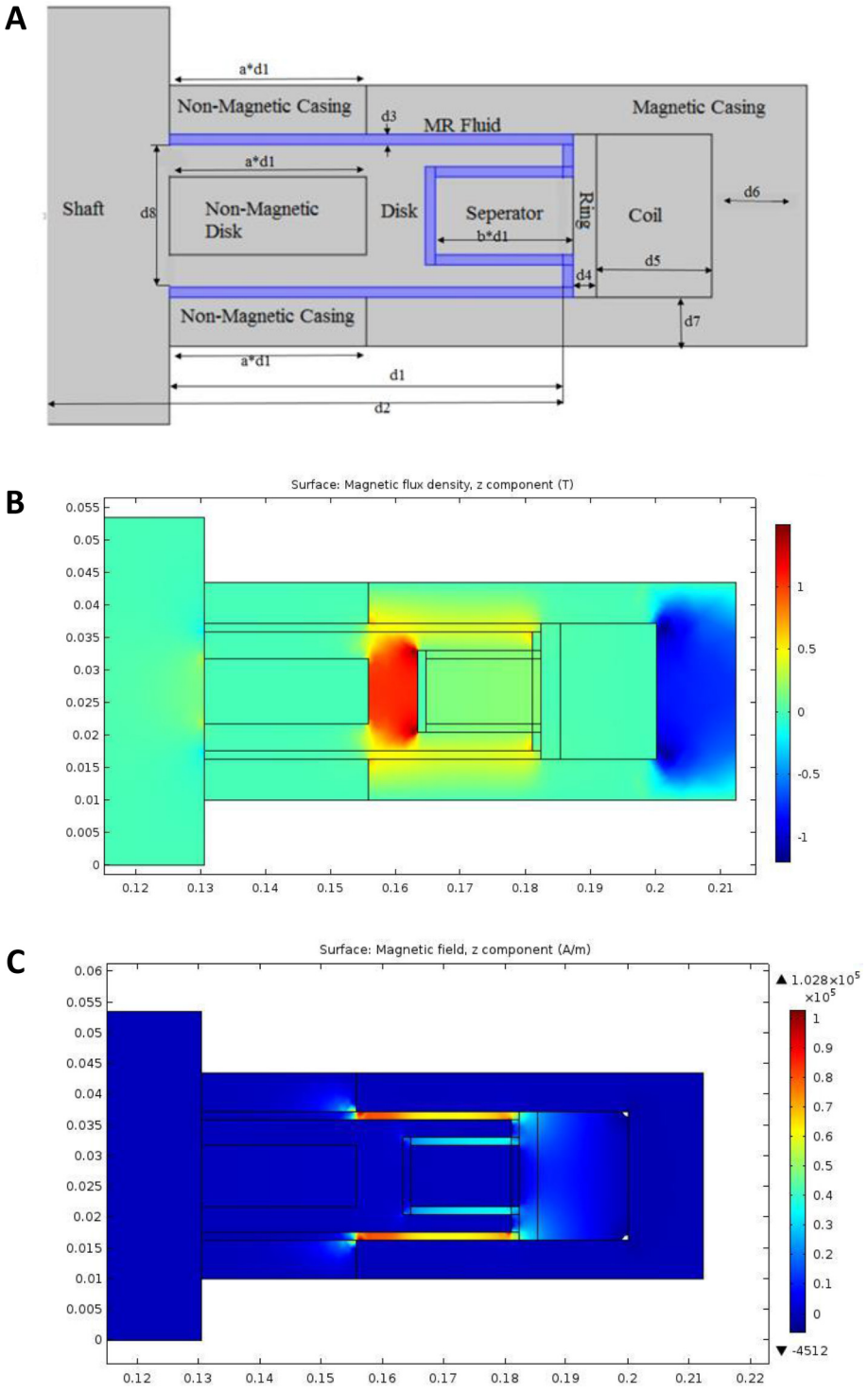

Fig. 3. Validation of the numerical method. (A) Reproduce schematic model of the MR brake presented by Assadsangabi et al. [21], (B) z component of magnetic flux density (Hz), (C) z component of magnetic field intensity (Bz).

selected to find the efficient prototype (Fig. 6A). Table 4 shows lower and upper bound for the optimized parameters. These values are selected in a way to have no significant changes in MR brake weight proposed in reference [21]. The optimum values for these parameters were detected after iterations and magnetic torque was calculated as the objective for these optimization iterations (Fig. 6B). The optimum dimensions are presented in Table 5 and Figure 5C shows magnetic flux distribution for the model with these dimensions. According to the Table 5, magnetic torque was obtained near 215.75 N m which is almost 73% more than previous configurations

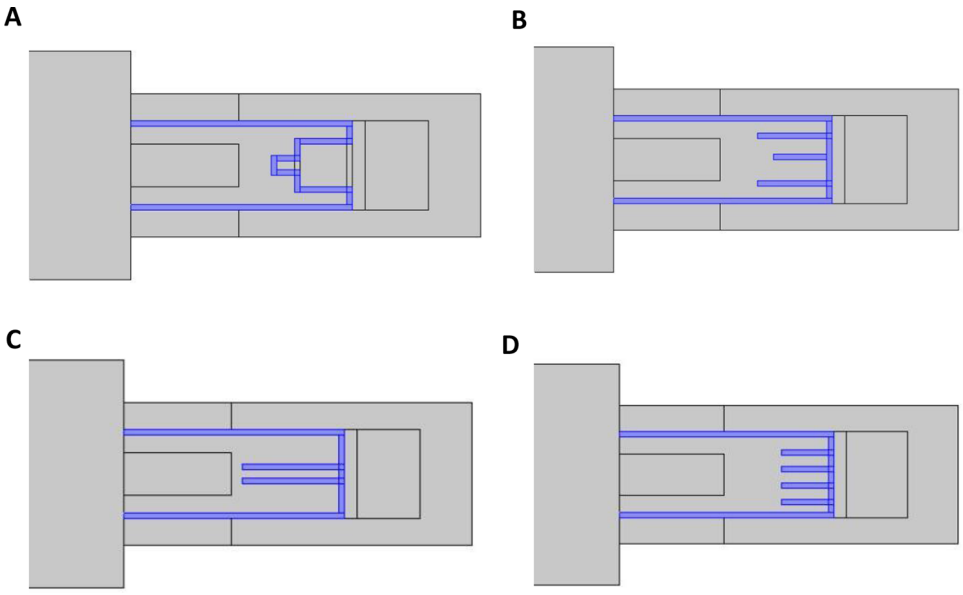

Fig. 4. Different studied layouts of the new MR brake.

Table 3. Magnetic torque of different layouts.

Layout	Magnetic torque (N m)
Main design	125.02
a	113.68
b	147.07
c	164.38
d	126.54

Table 4. Upper and lower values for parameters.

Parameters	Bound
$d1$	0.0013–0.0031
$d2$	0.005–0.013
$d3$	0.009–0.0264

(125.06 N m). It should be mentioned that amount of MR fluid increases in the new design which leads to produce more torque within near the same dimensions. It should be noted that for optimization, the upper and lower bounds of the distance between disks were selected in a way to be almost similar to reference [21] which would be possible for manufacturing process. In addition, the present layout has ease fabrication process. In order to build such disk, only two cuts should be machined on the outer disk edge which address the need of using a separator.

Table 5. Optimization parameters.

Parameters	Optimum values
Magnetic torque	215.75 (N m)
$d1$	0.0013
$d2$	0.00334
$d3$	0.0264

4 Conclusion

In the present study, FEM was employed in order to propose a new MR brake. The numerical procedure was validated by the available data in the literature. Then, different models were simulated and the most efficient ones was selected. This model was also optimized using Nelder–Mead optimization algorithm. The most important outcomes of this study were:

– Increasing the number of immersed disks in the MR fluid not necessarily enhances braking efficiency and the MR fluid gap dimensions should be also determined precisely.
– The proposed magnetic torque in the literature (125.06 N m) [21] could be generated by the present configuration with half of the coil current which was used previously.
– Distance between the MR fluid gaps was also one of the influential parameters on the brake effectiveness.
– Nelder–Mead optimization confirmed that when the length of the disks increases, the efficiency increases.

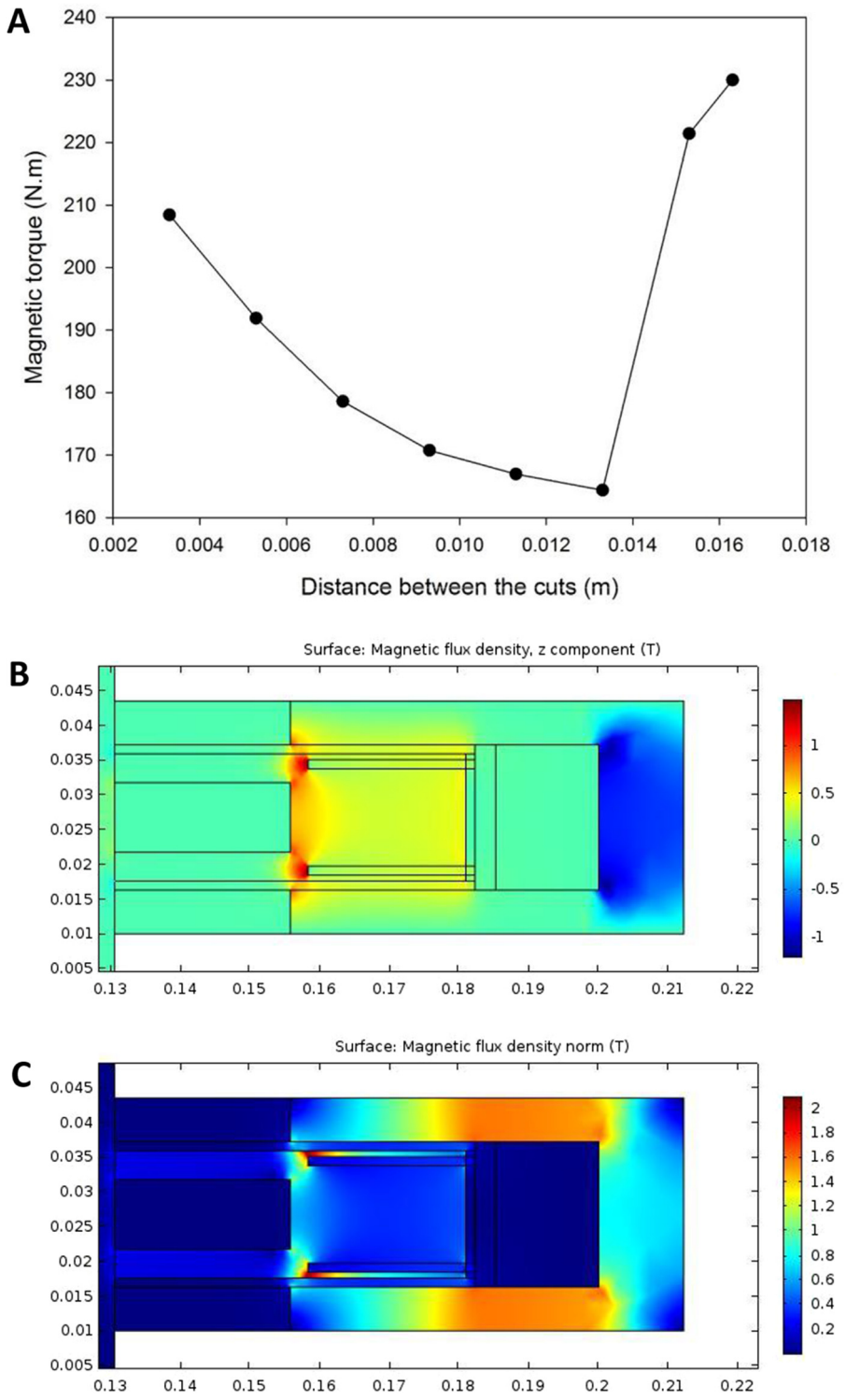

Fig. 5. Effects of the distance between the cuts on the brake efficiency. (A) Magnetic torque regarding cut distances, (B) z component of magnetic flux density (Hz), (C) z component of magnetic field intensity (Bz).

These results proved that the proposed MR brake in the present study enhanced braking efficiency about 73%. Also, the new configuration has lower fabrication costs, because the MR fluid gaps can be machined on the edge of the disk and the separator can be omitted from the previous designs.

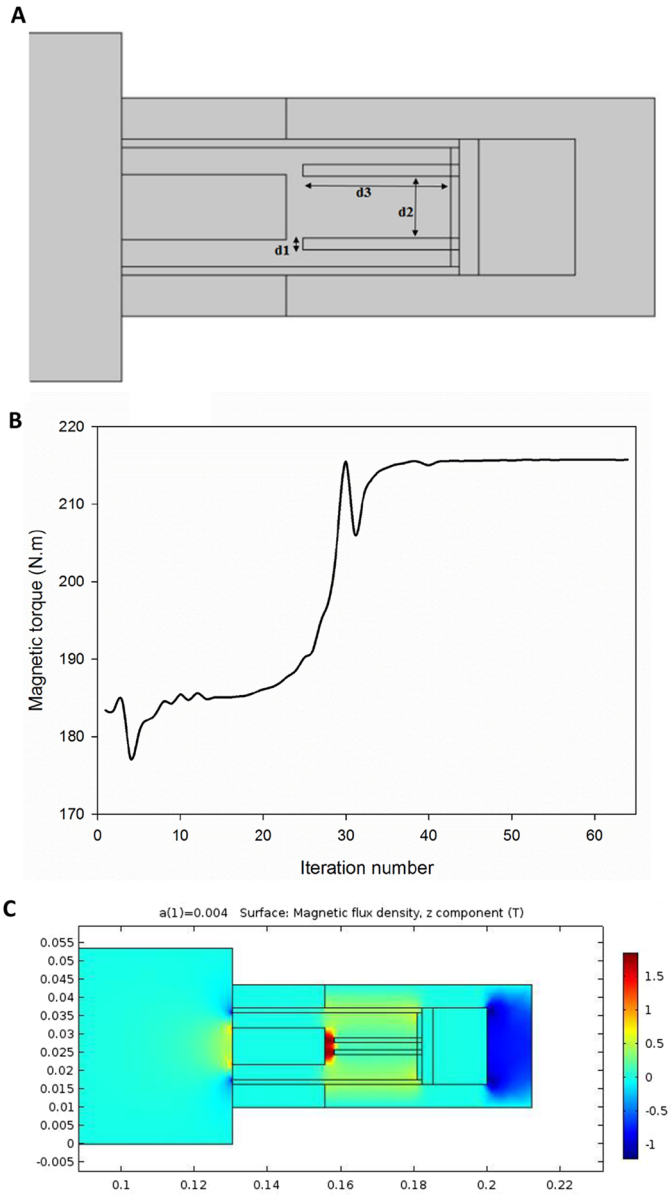

Fig. 6. Optimization of the brake with two MR fluid gaps. (A) Control variables, (B) iteration number, (C) magnetic flux density for the optimized MR brake.

Nomenclature

$\tau_y(H)$	Yield stress due to the applied magnetic field (N/m^2)
μ_p	Plastic viscosity (Pa s)
$\dot{\gamma}$	Shear–strain rate (1/s)
r	Radius of the disk (m)
ω	Angular velocity (Rad/s)
δ	MRF gap (m)
H	Magnetic field intensity (T)
J	Current density (A/m^2)
μ_o	Permeability of free space (N/A^2)
μ_r	Relative permeability

Acknowledgments. The author appreciates Mr. Mohammad Karim Dehghan Manshadi for his advises in models and simulations.

References

[1] M. Kciuk, R. Turczyn, Properties and application of magnetorheological fluids, J. Achiev. Mater. Manuf. Eng. **18**, 127–130 (2006)
[2] M. Ashtiani, S. Hashemabadi, A. Ghaffari, A review on the magnetorheological fluid preparation and stabilization, J. Magn. Magn. Mater. **374**, 716–730 (2015)
[3] J. de Vicente, D.J. Klingenberg, R. Hidalgo-Alvarez, Magnetorheological fluids: a review, Soft Matter **7**, 3701–3710 (2011)
[4] F. Gao, Y.-N. Liu, W.-H. Liao, Optimal design of a magnetorheological damper used in smart prosthetic knees, Smart Mater. Struct. **26**, 035034 (2017)
[5] C. Sarkar et al., Experimental studies on magnetorheological brake containing plane, holed and slotted discs, Ind. Lubr. Tribol. **69**, 116–122 (2017)
[6] J. Viau et al., Tendon-driven manipulator actuated by magnetorheological clutches exhibiting both high-power and soft motion capabilities, IEEE/ASME Trans. Mechatron. **22**, 561–571 (2017)
[7] G. Hu, M. Liao, W. Li, Analysis of a compact annular-radial-orifice flow magnetorheological valve and evaluation of its performance, J. Intell. Mater. Syst. Struct. **28**, 1322–1333 (2017)
[8] M. Chen et al., Design and fabrication of a novel magneto-rheological finishing process for small concave surfaces using small ball-end permanent-magnet polishing head, Int. J. Adv. Manuf. Technol. **83**, 823–834 (2016)
[9] D. Severin, S. Dörsch, Friction mechanism in industrial brakes, Wear **249**, 771–779 (2001)
[10] V.R. Bommadevara, A new electro-magnetic brake for actuator locking mechanism in aerospace vehicle, in 2017 IEEE International Magnetics Conference (INTERMAG), 2017, pp. 1–1
[11] D. Khachane, A. Shrivastav, Antilock braking system and its advancement, 2016
[12] R.L. Mott, Machine elements in mechanical design. Prentice Hall, NJ, 1999
[13] K. Lijesh, D. Kumar, H. Hirani, Effect of disc hardness on MR brake performance, Eng. Fail. Anal. **74**, 228–238 (2017)
[14] D. Senkal, H. Gurocak, Haptic joystick with hybrid actuator using air muscles and spherical MR-brake, Mechatronics **21**, 951–960 (2011)
[15] J. Blake, H.B. Gurocak, Haptic glove with MR brakes for virtual reality, IEEE/ASME Trans. Mechatron. **14**, 606–615 (2009)
[16] S.R. Patil, K.P. Powar, S.M. Sawant, Thermal analysis of magnetorheological brake for automotive application, Appl. Therm. Eng. **98**, 238–245 (2016)
[17] J.-H. Lee et al., Tension control of wire rope in winch spooler using magneto rheological brake, Int. J. Precis. Eng. Manuf. **17**, 157–162 (2016)
[18] J.J. Lima, R.T. Rocha, F.C. Janzen, A.M. Tusset, D.G. Bassinello, J.M. Balthazar, Position control of a manipulator robotic arm considering flexible joints driven by a DC motor and a controlled torque by a MR-brake, in ASME 2016 International Mechanical Engineering Congress and Exposition, Phoenix, Arizona, USA, November 11–17, 2016

[19] C. Sarkar, H. Hirani, Conceptual Design of Magneto-rheological Brake using TK Solver, Int. J. Curr. Eng. Technol. **5**, 990–993 (2015)
[20] E.J. Park, L.F. da Luz, A. Suleman, Multidisciplinary design optimization of an automotive magnetorheological brake design, Comput. Struct. **86**, 207–216 (2008)
[21] B. Assadsangabi et al., Optimization and design of disk-type MR brakes, Int. J. Automot. Technol. **12**, 921–932 (2011)
[22] W. Zhou, C.-M. Chew, G.-S. Hong, Development of a compact double-disk magneto-rheological fluid brake, Robotica **25**, 493–500 (2007)
[23] D. Wang, Y. Hou, Z. Tian, A novel high-torque magneto-rheological brake with a water cooling method for heat dissipation, Smart Mater. Struct. **22**, 025019 (2013)
[24] N. Wang et al., Effect of surface texture and working gap on the braking performance of the magnetorheological fluid brake, Smart Mater. Struct. **25**, 105026 (2016)
[25] R.S. Lydia et al. Design and development of coil casing MRF brake system, in: MATEC Web of Conferences, EDP Sciences, Paris, 2017
[26] A. Younis et al., Application of SEUMRE global optimization algorithm in automotive magnetorheological brake design, Struct. Multidiscipl. Optim. **44**, 761–772 (2011)
[27] B.K. Kumbhar, S.R. Patil, S.M. Sawant, Synthesis and characterization of magneto-rheological (MR) fluids for MR brake application, Eng. Sci. Technol. Int. J. **18**, 432–438 (2015)
[28] K. Karakoc, E.J. Park, A. Suleman, Design considerations for an automotive magnetorheological brake, Mechatronics **18**, 434–447 (2008)
[29] Q. Nguyen, V. Lang, S. Choi, Optimal design and selection of magneto-rheological brake types based on braking torque and mass, Smart Mater. Struct. **24**, 067001 (2015)
[30] M. Hajiyan et al., A new design of magnetorheological fluid based braking system using genetic algorithm optimization, Int. J. Mech. Mater. Des. **12**, 449–462 (2016)
[31] H. Shamieh, R. Sedaghati, Design optimization of a magneto-rheological fluid brake for vehicle applications, in: ASME 2016 Conference on Smart Materials, Adaptive Structures and Intelligent Systems, American Society of Mechanical Engineers, NY, 2016
[32] G. Marannano, G. Virzì Mariotti, Č. Duboka, Preliminary design of a magnetorheological brake for automotive use, in Science and motor vehicles, international automotive conference 2011, pp. 1–20
[33] J. Wu et al., Design and modelling of a novel multilayered cylindrical magnetorheological brake, Int. J. Appl. Electromagn. Mech. **53**, 29–50 (2017)
[34] W. Li, H. Du, Design and experimental evaluation of a magnetorheological brake, Int. J. Adv. Manuf. Technol. **21**, 508–515 (2003)
[35] Q. Nguyen, S. Choi, Optimal design of an automotive magnetorheological brake considering geometric dimensions and zero-field friction heat, Smart Mater. Struct. **19**, 115024 (2010)
[36] K.Y. Lee et al., Heuristic optimization techniques, in: Advanced Solutions in Power Systems: HVDC, FACTS, and Artificial Intelligence: HVDC, FACTS, and Artificial Intelligence, Wiley, NJ, 2016, pp. 931–984
[37] K.Y. Lee, M.A. El-Sharkawi, Modern heuristic optimization techniques: theory and applications to power systems, Vol. 39, John Wiley & Sons, NJ, 2008
[38] M.K. Sarakhsi, S.F. Ghomi, B. Karimi, A new hybrid algorithm of scatter search and Nelder-Mead algorithms to optimize joint economic lot sizing problem, J. Comput. Appl. Math. **292**, 387–401 (2016)
[39] K. Klein, J. Neira, Nelder-mead simplex optimization routine for large-scale problems: a distributed memory implementation, Comput. Econ. **43**, 447–461 (2014)
[40] R. Kamali, M.K.D. Manshadi, A. Mansoorifar, Numerical analysis of non Newtonian fluid flow in a low voltage cascade electroosmotic micropump, Microsyst. Technol. **22**, 2901–2907 (2016)
[41] R. Kamali, A. Mansoorifar, M.D. Manshadi, Effect of baffle geometry on mixing performance in the passive micromixers, Iran. J. Sci. Technol. Trans. Mech. Eng. **38**, 351 (2014)
[42] R. Kamali, M.K.D. Manshadi, Numerical simulation of the leaky dielectric microdroplet generation in electric fields, Int. J. Mod. Phys. C **27**, 1650012 (2016)
[43] M.K. Dehghan, Manshadi et al., Electroosmotic micropump for lab-on-a-chip biomedical applications, Int. J. Numer. Model. Electron. Netw. Devices Fields **29**, 845–858 (2016)
[44] M.K.D. Manshadi et al., Numerical analysis of non-uniform electric field effects on induced charge electrokinetics flow with application in micromixers, J. Micromech. Microeng. **29**, 035016 (2019)

Cite this article as: Y. Bazargan-Lari, Design and shape optimization of MR brakes using Nelder–Mead optimization algorithm, Mechanics & Industry **20**, 602 (2019)